Journal of Materials Chemistry A

ROYAL SOCIETY OF CHEMISTRY

PAPER

View Article Online
View Journal

Cite this: DOI: 10.1039/d5ta01329a

Monodisperse fluorinated 3D covalent organic frameworks for enhanced adsorption and extraction of perfluorocarboxylic acids†

Xu-Qin Ran,[bd] Can Zhu,[b] Qian-Ying Mao,[b] Shu-Ting Xu,[ab] Shuang-Ping Liu,[a] Peng Gu,[d] Yun Jiang,[d] Xiu-Ping Yan[abc] and Hai-Long Qian[*ab]

Advancements in covalent organic frameworks (COFs) in the field of adsorption and extraction are always limited by their non-uniform and irregularly aggregated morphology. Herein, we pioneer the preparation of monodisperse COFs with a regular shape and further explore their adsorption and extraction capabilities. As a proof of concept, a new monodisperse fluorinated 3D COF, named M-TAM-TFTA, featuring a nonpolar structure and uniform size and shape, is selected as the model COF for the adsorption and extraction of perfluorocarboxylic acids (PFCAs). M-TAM-TFTA, consisting of tetra(4-anilyl)methane (TAM) and 2,3,5,6-tetrafluoroterephthalaldehyde (TFTA), exhibits higher adsorption capacity (554.9 mg g^{-1}) and faster adsorption kinetics (5 min) compared to the same composition aggregated 3D COF A-TAM-TFTA as well as diverse reported materials. This remarkable adsorption performance of M-TAM-TFTA for PFCAs is proved to be dominantly caused by its lower mass transfer resistance structure and multiple specific interactions including F–F, hydrophobic, electrostatic and H-bonding interactions. M-TAM-TFTA is further applied to develop a probe nanoelectrospray ionization mass spectrometry (PESI-MS) method for direct and precise determination of PFCAs with a wide linear range (0.5–5000 ng L^{-1}) and low limits of detection (0.08–0.46 ng L^{-1}). This study provides robust support for the great potential of monodisperse COFs as adsorbents for the treatment of contaminants in complex samples.

Received 18th February 2025
Accepted 31st March 2025

DOI: 10.1039/d5ta01329a

rsc.li/materials-a

1 Introduction

Covalent organic frameworks (COFs) are crystalline and covalent bond-linked organic polymers with extended two-dimensional (2D) or three-dimensional (3D) structures, offering high surface areas and great stability.[1–3] COFs are well known for their predictable periodic porous structures, which arise from the strong modifiability of monomers, making them highly promising for a wide range of adsorption applications.[4–8] For instance, the topology, pore size, and functionality of COFs can be customized through the design and modification of monomers according to specific target structures and properties.[9–11] Furthermore, COFs can be composited with many other materials, including magnetic nanoparticles, spherical silica, and solid nanopores, enabling multifunctional integration for highly selective and efficient adsorption.[12–17]

Although COFs have already made significant advancements in the field of adsorption and extraction, they often exhibit aggregated states with an irregular morphology due to the rapid condensation rate under high-temperature and high-pressure conditions.[18,19] Non-uniformly aggregated COFs (A-COFs) would significantly hinder their adsorption and extraction performance. Monodisperse materials, referring to materials that are uniform in size, shape, and mass, have been proven to enhance the selectivity and conversion rates of reactions in catalysis, increase permeation flux in separation, and facilitate precise drug release and targeted delivery in the pharmaceutical field.[20–24] Monodisperse COFs (M-COFs) are theoretically more favorable and advanced in adsorption and extraction than A-COFs, but the practical potential of M-COFs as adsorbents has not yet been explored.

Lately, diverse strategies have been developed to regulate the polymerization and crystallization process during the formation of COFs, mainly falling into three categories: (I) employment of reaction inhibitors to reduce the polymerization rate. For instance, aniline always serves as an efficient nucleation inhibitor for the Schiff-base reaction in the preparation of imine single-crystal COFs.[25,26] (II) Introducing specific small molecules or polymers as templating agents to guide the growth of COFs in

[a]State Key Laboratory of Food Science and Resources, Jiangnan University, Wuxi 214122, China. E-mail: hlqian@jiangnan.edu.cn

[b]Institute of Analytical Food Safety, School of Food Science and Technology, Jiangnan University, Wuxi 214122, China

[c]Key Laboratory of Synthetic and Biological Colloids, Ministry of Education, School of Chemical and Material Engineering, Jiangnan University, Wuxi 214122, China

[d]Department of Light Chemical Engineering, Jiangnan University, Wuxi 214122, PR China

† Electronic supplementary information (ESI) available. See DOI: https://doi.org/10.1039/d5ta01329a

a predetermined manner. The negatively charged polymer poly(sodium 4-styrenesulfonate) can guide the assembly, polymerization, and crystallization of protonated monomers, resulting in the formation of oriented large single-crystal 2D COFs.[27] (III) Application of dynamic barriers to separate monomers regulating the crystallization rate. For example, palmitoyl glycine (C_{16}-GlyA) was employed to create hydrophobic cavities in water to limit the condensation rate of COF monomers.[28] Although these methods were originally developed for the synthesis of single-crystalline COFs, they also make the preparation of M-COFs possible, further enabling the investigation of the adsorption potential of M-COFs.

Herein, we pioneeringly designed to synthesize monodisperse COFs and further explored their adsorption capabilities. Perfluorocarboxylic acids (PFCAs), as emerging pollutants, have raised significant concern due to their persistence, bioaccumulation, and toxicity. As a proof of concept, a monodisperse fluorinated COF (M-TAM-TFTA) with a non-polar 3D structure, consisting of 2,3,5,6-tetrafluoroterephthalaldehyde (TFTA) and tetra(4-anilyl)methane (TAM), was selected as the model COF, and its adsorption efficiency for PFCAs was assessed in-depth. Additionally, the proposed M-COF was further applied in probe nanoelectrospray ionization mass spectrometry (PESI-MS) to explore its practical adsorption potential in real samples.

2 Experimental

2.1 Materials and chemicals

All chemicals are commercially available and used directly. TAM and TFTA were bought from CHEMSOON Co., Ltd (Shanghai, China). C_{16}-GlyA, *p*-toluenesulfonic acid monohydrate (PTSA), acetonitrile (CH_3CN), acetic acid (HAc), sodium hydroxide (NaOH), HCl, tetrahydrofuran (THF), and PFCAs were purchased from Aladdin Chemistry Co., Ltd (Shanghai, China). Perfluoro-*n*-(1,2,3,4-$^{13}C_4$) octanoic acid ($^{13}C_4$-PFOA) was achieved from Wellington Laboratories Inc (Ontario, Canada). Methanol was bought from Fisher Chemical (Shanghai, China). Ultrapure water was obtained from Wahaha Foods Co., Ltd (Shanghai, China). The stainless needle (diameter: 0.25 mm and length: 40 mm) was purchased from Huaer Medical Instrument Co., Ltd (Hebei, China). Water samples were collected from Lihu and Taihu Lakes with no preliminary treatment before use.

2.2 Preparation of the monodisperse 3D COF

Typically, amino acid derivatives C_{16}-GlyA (0.2 mmol) and 0.2 mol per L NaOH (1 mL) were mixed with 15 mL water at 50 °C and sonicated for 20 min to obtain a uniform emulsion. Subsequently, a 0.2 mol per L PTSA (4.0 mL) solution containing TAM (0.05 mmol) was added to the emulsion under sonication for an additional 10 min. Next, TFTA (0.1 mmol) was added and the mixture was continuously sonicated for another 10 min. The final mixture was sealed and left undisturbed at 50 °C for 4 days. The obtained product was collected by centrifugation, washed three times with water and THF, and then immersed in THF for 24 h, followed by drying for 12 h at 60 °C to afford M-TAM-TFTA.

2.3 Preparation of the aggregated 3D COF

Typically, TAM (0.05 mmol) and TFTA (0.1 mmol) were mixed with 5 mL CH_3CN under ultrasonic conditions for 5 min. After the addition of 2 mL HAc (6 mol L^{-1}), the mixture was further sonicated for 15 min and left undisturbed at 50 °C for 24 h. The resulting product was collected *via* centrifugation, washed three times with water and THF, and then immersed in THF for 24 h, followed by drying for 12 h at 60 °C to yield aggregated A-TAM-TFTA.

2.4 Procedure of M-TAM-TFTA based PESI-MS

The M-TAM-TFTA based probe was first cleaned with water and methanol and then immersed in 1.5 mL prepared samples or standard solution while stirring for 2 min and finally rinsed with ultrapure water for 10 s. Subsequently, the probe was fixed on a homemade device detailed in our prior study[29] and then methanol at a flow rate of 20 μL min^{-1} was pumped to elute the probe. Next, a voltage of −3.2 kV was applied to the M-TAM-TFTA based probe to produce a charged spray of the adsorbed PFCAs for direct MS analysis. The probe was rinsed with methanol and water to enable its reuse.

3 Results and discussion

3.1 Preparation and characterization of the monodisperse 3D COF

The tetrahedral configuration of TAM enables the formation of a nonpolar 3D structure, while linear TFTA can introduce abundant fluorine groups for F–F interactions. This combination of a nonpolar 3D architecture functionalized with specific interactions is expected to achieve selective enhanced adsorption of PFCAs.[30] Therefore, TAM and TFTA were selected as monomers to construct the proof-of-concept monodisperse COF, referring to the preparation strategy for single-crystalline 3D COFs.[28] C_{16}-GlyA was applied to self-assemble supramolecular micelles under alkaline conditions, which can prevent TFTA from polymerizing with the TAM protonated by PTSA, thereby controlling the crystallization rate to obtain the monodisperse nonpolar fluorinated 3D COF, named M-TAM-TFTA (Fig. 1). In contrast, the same composite 3D COF but in the aggregated state (A-TAM-TFTA) was also prepared in CH_3CN with HAc as the catalyst.

M-TAM-TFTA showed several prominent diffraction peaks at 8.6°, 12.2°, 17.2°, 18.5°, 20.4°, and 23.9°, indicating its long-range ordered crystalline structure (Fig. 2a). These peaks appeared at positions similar to those of the simulated powder X-ray diffraction (PXRD) pattern generated using the dia-C7 structure (Fig. 2b–d). Further refinement using experimental PXRD data produced more specific simulated unit cell parameters for M-TAM-TFTA: space group $I41/A$, $a = b = 20.5537$ Å, $c = 8.8063$ Å, and $\alpha = \beta = \gamma = 90°$ (Fig. 2e and Table S1†). In contrast, A-TAM-TFTA showed poor crystallinity due to its low resolution of PXRD patterns (Fig. S1†).

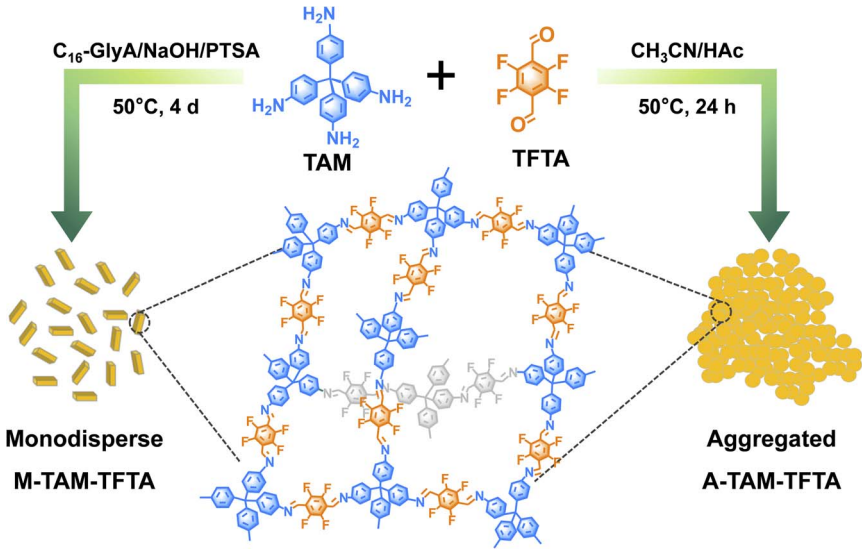

Fig. 1 Schematic illustration for the preparation of M-TAM-TFTA and A-TAM-TFTA.

Fourier transform infrared (FTIR) spectra of both M-TAM-TFTA and A-TAM-TFTA showed an imine peak at 1620 cm^{-1}, indicating the successful condensation of COF monomers (Fig. 2f). The evident FTIR peaks at 1299 and 1300 cm^{-1}, assigned to the C–F group, as well as the presence of the F 1s peak in the wide X-ray photoelectron spectroscopy (XPS) scan spectra can fully reveal the rich fluorine groups in both M-TAM-TFTA and A-TAM-TFTA (Fig. S2†). More importantly, the highly similar FTIR spectra confirmed the identical composition of M-TAM-TFTA and A-TAM-TFTA. Energy dispersive X-ray spectroscopy (EDS) elemental mapping images showed the uniform distribution of F element in M-TAM-TFTA (Fig. S3†).

Scanning electron microscope (SEM) and transmission electron microscope (TEM) images directly showed the monodispersity of rod-like M-TAM-TFTA (Fig. 2g and S4†) with a size of 10.73 ± 1.87 μm. In contrast, A-TAM-TFTA showed irregular morphology and uniform size (Fig. S5 and S6†). Moreover, the Brunauer–Emmett–Teller (BET) surface area of M-TAM-TFTA (260 $m^2\ g^{-1}$) was slightly larger than that of A-TAM-TFTA (180 $m^2\ g^{-1}$) (Fig. S7†).

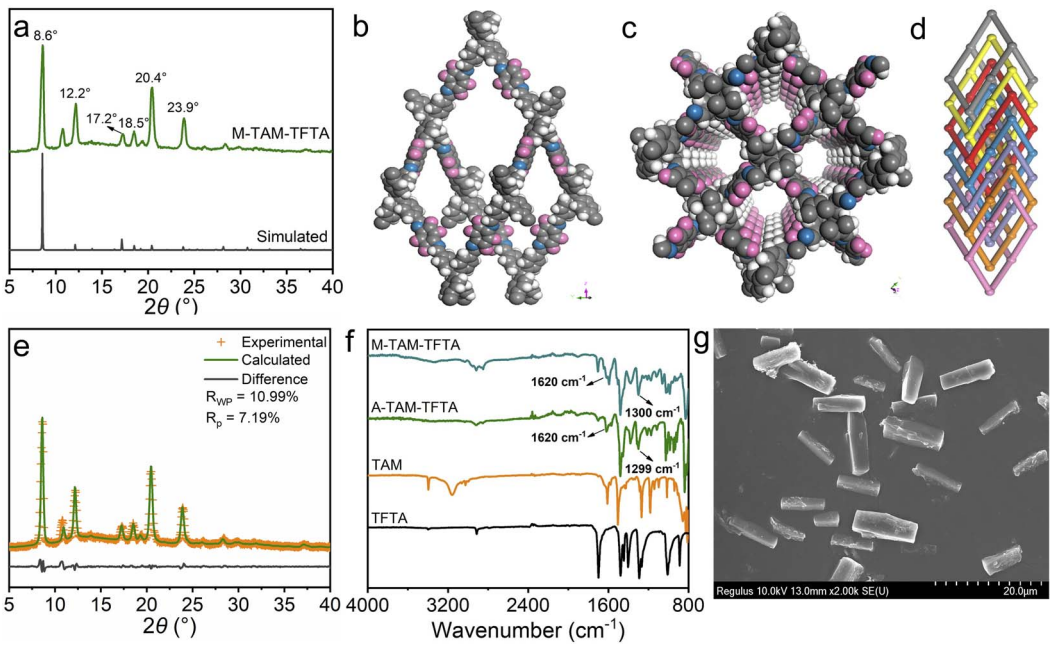

Fig. 2 (a) Experimental and simulated PXRD patterns of M-TAM-TFTA. Structural representation of (b) the crystal unit and (c) the 3D porous framework of M-TAM-TFTA in a space-filling model (gray C, white H, blue N, and pink F). (d) 7-fold interpenetrated diamond network (dia-C7) of M-TAM-TFTA. (e) Refinement result of M-TAM-TFTA. (f) FTIR spectra of TAM, TFTA, M-TAM-TFTA and A-TAM-TFTA. (g) SEM image of M-TAM-TFTA.

3.2 Adsorption performance

Perfluorooctanoic acid (PFOA), one of the explicitly prohibited PFCAs, was selected as the model analyte to evaluate the adsorption performance of the prepared monodisperse 3D COFs for PFCAs. The highest equilibrium adsorption capacity (q_e) of both M-TAM-TFTA and A-TAM-TFTA for PFOA was obtained at pH 5, indicating that pH 5 is the optimal condition for adsorption (Fig. S8†). The adsorption kinetics of M-TAM-TFTA and A-TAM-TFTA were better fitted with the pseudo-second-order model than the pseudo-first-order model (Fig. S9, S10 and Table S2†), demonstrating the involvement of electron sharing or transfer during adsorption.[31] The equilibrium time for PFOA adsorption on M-TAM-TFTA (5 min) was significantly faster than that on A-TAM-TFTA (15 min) (Fig. 3a and S11†). The adsorption isotherms for PFOA on both M-TAM-TFTA and A-TAM-TFTA can be better described by the Langmuir model than the Freundlich model, indicating monolayer adsorption (Fig. 3b and Table S3†).[32] The calculated maximum adsorption capacity (q_m) of M-TAM-TFTA for PFOA (554.9 mg g^{-1}) was also evidently larger than that of A-TAM-TFTA (350.8 mg g^{-1}).

According to the rate coefficient and q_e fitted using the pseudo-second-order model, the calculated mass transfer resistance (R_m) for the adsorption of PFOA on M-TAM-TFTA can be as low as 0.0016 min mg^{-1}, due to its uniform mass and more open active sites. In contrast, the R_m of PFOA on A-TAM-TFTA was significantly one order of magnitude higher (0.0107 min mg^{-1}), indicating the dominant role of R_m contributing to the excellent adsorption performance of monodisperse COFs (Table S2†). Notably, the proposed M-TAM-TFTA exhibited better adsorption kinetics and capacity for PFOA than not only A-TAM-TFTA, but also diverse previously reported materials, making M-TAM-TFTA promising for the extraction or removal of PFCAs (Table S4†).

3.3 Adsorption mechanism

The contact angle of M-TAM-TFTA (105.3°) verified their hydrophobic structures, which can enable hydrophobic interaction with PFOA (Fig. S12†). Compared to the XPS spectra of M-TAM-TFTA, a new peak at 689.2 eV, assigned to the F···F, appeared after the adsorption of PFOA (Fig. 3c), confirming the presence of F–F interactions between M-TAM-TFTA and PFOA. Furthermore, density functional theory (DFT) calculations were performed using a typical fragment of M-TAM-TFTA (X-TFTA) as a theoretical model to study the underlying adsorption mechanisms. The van der Waals surfaces of X-TFTA and PFOA, mapped with electrostatic potentials (ESPs), illustrate the positive potential near the benzene ring of X-TFTA and negative potential near the carbonyl group of PFOA, indicating the feasibility of electrostatic interactions between TAM-TFTA and PFOA (Fig. 3d). The spatial position values of sign $(\lambda_2)\rho$ in the reduced density gradient function (RDG) color-filled isosurface map located in the range of −0.05 to −0.01 indicate attractive interactions between X-TFTA and PFOA rather than repulsive effects (Fig. 3e). Furthermore, the independent gradient model based on Hirshfeld partition (IGMH) images of X-TFTA and PFOA reveals that the prominent attractive effects tended to be more inclined towards van der Waals force and weak interaction, referring to F–F interaction and H-bonding interaction (Fig. 3f).

3.4 Development of monodisperse 3D COF based PESI-MS

The excellent adsorption performance of M-TAM-TFTA highlights the practical potential of monodisperse COFs for the determination of PFCAs including perfluorohexanoic acid (PFHxA), perfluoroheptanoic acid (PFHpA), perfluorooctanoic acid (PFOA), perfluorononanoic acid (PFNA), perfluorodecanoic

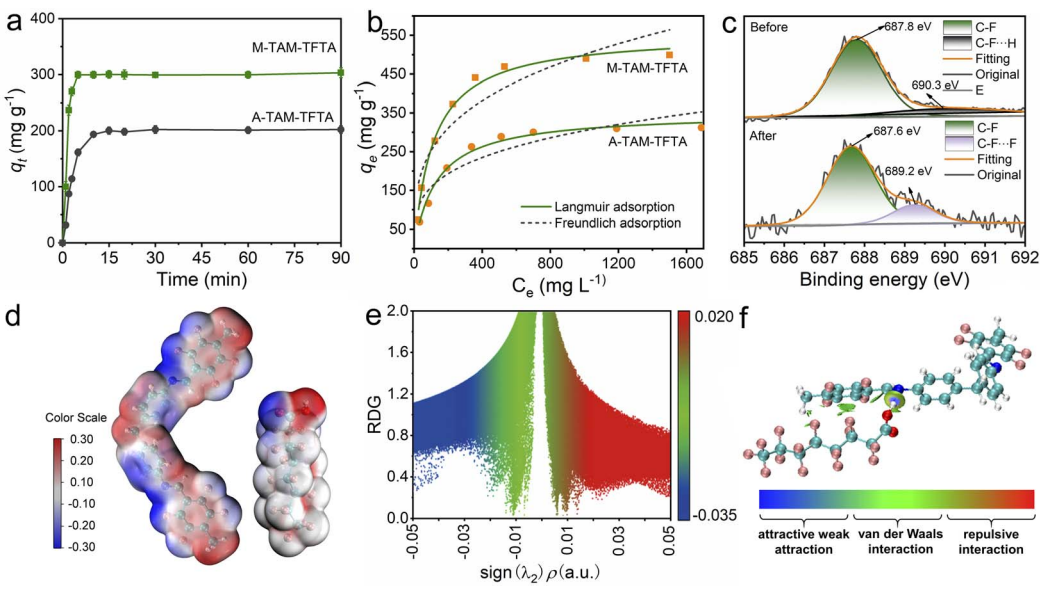

Fig. 3 (a) Effect of time on the adsorption of PFOA on M-TAM-TFTA and A-TAM-TFTA. (b) Adsorption isotherms of PFOA (100–2000 mg L^{-1}) on M-TAM-TFTA and A-TAM-TFTA. (c) F 1s XPS spectra of M-TAM-TFTA before and after adsorption of PFOA. (d) van der Waals surfaces of X-TFTA and PFOA. (e) RDG color-filled isosurface map for the interactions between X-TAM and PFOA. (f) IGMH image of X-TFTA and PFOA in their optimal configuration.

acid (PFDA), and perfluoroundecanoic acid (PFUnDA) in real samples. Therefore, M-TAM-TFTA was further coated onto a stainless needle using a neutral silicone sealant to serve as a probe to enrich the PFCAs. The probe was then eluted with methanol and subsequently functioned as an ESI emitter after the application of high voltage to generate a charged spray of enriched PFCAs for direct MS analysis (Fig. 4a). SEM and EDS elemental mapping showed the uniform distribution of M-TAM-TFTA on the stainless needle surface (Fig. 4b, S13 and S14†), and the cross-sectional SEM image revealed that the thickness of the M-TAM-TFTA layer was approximately 25 μm (Fig. 4c).

Subsequently, the M-TAM-TFTA based probe was employed to couple with PESI-MS for the sensitive and rapid detection of six PFCAs including PFHxA, PFHpA, PFOA, PFNA, PFDA and PFUnDA. The optimized qualitative and quantitative ion pairs of the six PFCAs and $^{13}C_4$-PFOA (serving as an IS) in a multiple reaction monitoring (MRM) model are listed in Table S5.† Through monitoring the ratio of the quantitative ion intensity of PFCAs to the IS (I_A/I_{IS}), the extraction was found to be complete in 2 min, because of no significant change in I_A/I_{IS} after 2 min (Fig. 4d). No evident ions can be detected after elution with methanol at a flow rate of 20 μL min^{-1} for 1.5 min, demonstrating the complete elution of PFCAs from the M-TAM-TFTA based probe within 1.5 min (Fig. S15†).

The analysis of PFCA aqueous solution (0.1–10000 ng L^{-1}) spiked with 100 ng L^{-1} $^{13}C_4$-PFOA showed that I_A/I_{IS} exhibited a linear increase with the concentration of PFCAs in the range of 0.5–5000 ng L^{-1} ($R^2 \geq 0.999$). The calculated limits of detection (LODs, S/N = 3) and limits of quantification (LOQs, S/N = 10) of the developed M-TAM-TFTA based PESI-MS for the six PFCAs were 0.08–0.46 ng L^{-1} and 0.27–1.54 ng L^{-1}, respectively, which is much lower than the EPA limit for PFCAs in national drinking water (5 ng L^{-1}).[33] The relative standard deviation (RSD) of I_A/I_{IS} in six tests using the same probe ranged from 2.5% to 6.2%, while the RSD of I_A/I_{IS} using three different probes varied between 4.8% and 9.3%, indicating the reliable repeatability and reproducibility of the developed probe (Fig. S16 and Table S6†). After 50 cycles of extraction, no significant decline in I_A/I_{IS} for 1000 ng per L PFCAs was observed, nor was any significant change detected in the FTIR spectra of M-TAM-TFTA (Fig. S17 and S18†), indicating the good reusability of the M-TAM-TFTA based probe. The superiority in sensitivity and time efficiency makes the proposed M-TAM-TFTA based PESI-MS method desirable as an alternative method in the practical determination of PFCAs (Table S7†).

3.5 Analysis of real samples

The matrix factor (MF) of three real water samples ranged from 90.0% to 100.1%, demonstrating that M-TAM-TFTA can effectively eliminate matrix interference and the calibration curve established using pure water remains valid for actual water samples (Fig. S19†). Trace PFCAs can be detected in almost all three water samples. The concentrations of PFCAs in water samples I, II, and III were detected as follows: PFHxA at 27.3 ng L^{-1}, 10.0 ng L^{-1}, and 9.4 ng L^{-1}; PFOA at 8.0 ng L^{-1}, 6.2 ng L^{-1}, and 2.5 ng L^{-1}; PFNA at 9.7 ng L^{-1}, 15.5 ng L^{-1}, and 10.0 ng L^{-1}; and PFDA at 28.4 ng L^{-1}, 11.8 ng L^{-1}, and 5.3 ng L^{-1}, respectively. PFHpA and PFUnDA can only be found in water sample I (20.0 ng L^{-1}) and water sample III (8.8 ng L^{-1}), respectively. Furthermore, the three water samples were spiked with 100 ng per L PFCAs, and the obtained recoveries of M-TAM-TFTA based PESI-MS for these spiked samples varied from 89.5% to 104.7%, indicating the great accuracy of the

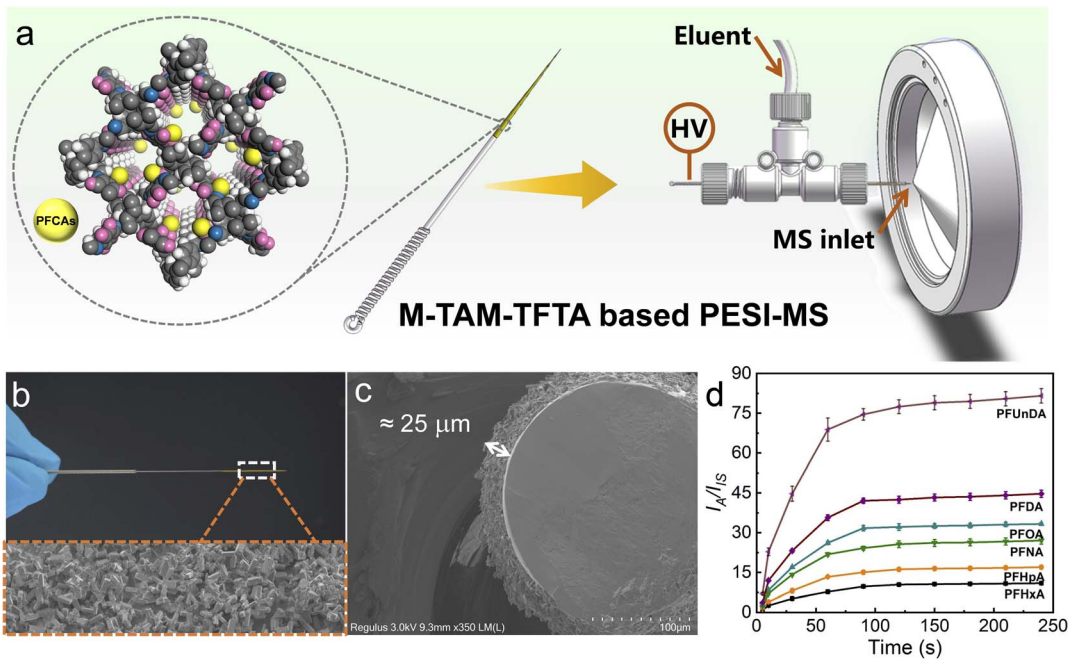

Fig. 4 (a) Schematic of M-TAM-TFTA based PESI-MS. (b) Photograph and SEM images of the M-TAM-TFTA based probe. (c) Cross-sectional SEM image of the M-TAM-TFTA based probe. (d) Effect of time on I_A/I_{IS} of PFCAs.

established method for the detection of PFCAs in environmental water samples (Table S8†).

4 Conclusions

In conclusion, we have first explored the adsorption potential of monodisperse COFs in this work. To this end, a monodisperse fluorinated 3D COF (M-TAM-TFTA) and aggregated A-TAM-TFTA were designed and synthesized to explore the adsorption of PFCAs. M-TAM-TFTA exhibited higher adsorption capacity and efficiency for PFCAs than A-TAM-TFTA as well as many reported adsorbents, which was proved to be dominantly caused by the lower mass transfer resistance of M-TAM-TFTA and multiple specific interactions for PFCAs including F–F, hydrophobic, electrostatic and H-bonding interactions. Furthermore, M-TAM-TFTA based ambient PESI-MS was established for the determination of six PFCAs in environmental water samples with a lower detection limit and wider linear range than many reported methods and the EPA limit. This work provides robust support for the great potential of M-COFs as adsorbents for the determination of contaminants in complex samples.

Data availability

All relevant data are within the manuscript and the ESI.†

Author contributions

Xu-Qin Ran: methodology, investigation, and writing – original draft. Can Zhu, Qian-Ying Mao and Shu-Ting Xu: methodology. Shuang-Ping Liu, Peng Gu, Yun Jiang and Xiu-Ping Yan: resources. Hai-Long Qian: conceptualization, methodology, writing – review & editing, resources, supervision, and funding acquisition.

Conflicts of interest

There are no conflicts to declare.

Acknowledgements

This work was supported by the National Natural Science Foundation of China (22376082 and 22422406), the "Fundamental Research Funds for the Central Universities" and the Jiangsu Funding Program for Excellent Postdoctoral Talent (No. 2023ZB116).

References

1 S. Das, H. Mabuchi, T. Irie, K. Sasaki, M. Nozaki, R. Tomioka, D. Wen, Y. Zhao, T. Ben and Y. Negishi, *Small*, 2024, **20**, 2307666.
2 F. Auras, L. Ascherl, V. Bon, S. M. Vornholt, S. Krause, M. Döblinger, D. Bessinger, S. Reuter, K. W. Chapman, S. Kaskel, R. H. Friend and T. Bein, *Nat. Chem.*, 2024, **16**, 1373–1380.
3 P. J. Waller, F. Gándara and O. M. Yaghi, *Acc. Chem. Res.*, 2015, **48**, 3053–3063.
4 E. Asayesh-Ardakani, M. Rahmani, A. Hosseinian, S.-B. Ghaffari and M.-H. Sarrafzadeh, *Coord. Chem. Rev.*, 2024, **518**, 216087.
5 S. Di, Q. Wu, C. Shi and S. Zhu, *ACS Appl. Mater. Interfaces*, 2023, **15**, 1827–1842.
6 Y. Lv, J. Ma, Z. Yu, S. Liu, G. Yang, Y. Liu, C. Lin, X. Ye, Y. Shi and M. Liu, *Water Res.*, 2023, **235**, 119892.
7 S. Di, M. Zhang, C. Shi and S. Zhu, *Environ. Pollut.*, 2023, **326**, 121475.
8 A. A. Aslam, A. Irshad, M. S. Nazir and M. Atif, *J. Cleaner Prod.*, 2023, **400**, 136737.
9 G. Li, Y. Wu, C. Zhong, Y. Yang and Z. Lin, *Chin. Chem. Lett.*, 2024, **35**, 108904.
10 Y. Zhao, X. Tao, B. Xu, W. Liu and S. Lin, *Adv. Funct. Mater.*, 2024, **34**, 2401895.
11 M. Liu, Q. Xu and G. Zeng, *Angew. Chem., Int. Ed.*, 2024, **63**, e202404886.
12 S. Y. Ding and W. Wang, *Chem. Soc. Rev.*, 2013, **42**, 548–568.
13 F. Wang, S. Xu, N. Wang, T. Fujita, S. Ning, Y. Wei and X. Wang, *J. Cleaner Prod.*, 2024, **474**, 143596.
14 T. Ning, S. Di, Z. Li, H. Zhang, Z. Peng, H. Yang, P. Chen, Y. Bao, Y. Zhai and S. Zhu, *Anal. Chim. Acta*, 2023, **1239**, 340615.
15 H. Guo, Y. Fang, J. Li, W. Feng, C. Fang and L. Zhu, *Nano Lett.*, 2024, **24**, 11438–11445.
16 H. Guo, J. Jiang, C. Fang and L. Zhu, *J. Mater. Chem. A*, 2023, **11**, 19374–19383.
17 R. Paz, H. Viltres, N. K. Gupta, V. Phung, S. Srinivasan, A. R. Rajabzadeh and C. Leyva, *Chemosphere*, 2023, **342**, 140145.
18 K. T. Tan, S. Ghosh, Z. Wang, F. Wen, D. Rodríguez-San-Miguel, J. Feng, N. Huang, W. Wang, F. Zamora, X. Feng, A. Thomas and D. Jiang, *Nat. Rev. Methods Primers*, 2023, **3**, 1.
19 Y. Wang, H. Wang, Y. Liu, M. Peng, H. Fan and H. Meng, *Chin. Chem. Lett.*, 2024, DOI: **10.1016/j.cclet.2024.110189**.
20 Y. Wang, X.-Q. Ran, C. Yang, H.-L. Qian and X.-P. Yan, *Anal. Chem.*, 2024, **96**, 5608–5614.
21 S. Deng, C.-X. Cui, L. Liu, L. Duan, J. Wang, Y. Zhang and L. Qu, *Chin. Chem. Lett.*, 2021, **31**, 1177–1180.
22 L. Qi, Y. Xiao, X. Fu, H. Yang, L. Fang, R. Xu, J. Ping, D. Han, Y. Jiang and X. Fang, *Small*, 2024, **20**, 2400238.
23 M. Zhang, M. Lu, T. Qiu, Q. Wang, Z. Chen, M. Deng, Y. Yang, Y. Yang, W. Li, Y. Ling and Y. Zhou, *Small*, 2023, **19**, 2301894.
24 L. Hu, G. Zhan, L. Zhao, J. Dai, X. Zou, J. Wang, W. Hou, H. Li, Y. Yao and L. Zhang, *Adv. Mater.*, 2024, **36**, 2400870.
25 A. Natraj, I. R. Landman, C. E. Pelkowski, D. W. Burke, S. Kewalramani and W. R. Dichtel, *J. Am. Chem. Soc.*, 2024, **146**, 16775–16786.
26 T. Q. Ma, E. A. Kapustin, S. X. Yin, L. Liang, Z. Y. Zhou, J. Niu, L. H. Li, Y. Y. Wang, J. Su, J. Li, X. G. Wang, W. D. Wang, W. Wang, J. L. Sun and O. M. Yaghi, *Science*, 2018, **361**, 48–52.

27 Z. Ou, B. Liang, Z. Liang, F. Tan, X. Dong, L. Gong, P. Zhao, H. Wang, Y. Zou, Y. Xia, X. Chen, W. Liu, H. Qi, U. Kaiser and Z. Zheng, *J. Am. Chem. Soc.*, 2022, **144**, 3233–3241.
28 Z. Zhou, L. Zhang, Y. Yang, I. J. Vitorica-Yrezabal, H. Wang, F. Tan, L. Gong, Y. Li, P. Chen, X. Dong, Z. Liang, J. Yang, C. Wang, Y. Hong, Y. Qiu, A. Gölzhäuser, X. Chen, H. Qi, S. Yang, W. Liu, J. Sun and Z. Zheng, *Nat. Chem.*, 2023, **15**, 841–847.
29 X.-Q. Ran, S.-T. Xu, H.-L. Qian and X.-P. Yan, *J. Hazard. Mater.*, 2023, **455**, 131584.
30 Q.-Y. Mao, X.-Q. Ran, S.-T. Xu, P. Gu, Y. Jiang, X.-P. Yan and H.-L. Qian, *Anal. Chem.*, 2025, **97**, 6312–6319.
31 A. Jrad, G. Das, N. Alkhatib, T. Prakasam, F. Benyettou, S. Varghese, F. Gándara, M. Olson, S. Kirmizialtin and A. Trabolsi, *Nat. Commun.*, 2024, **15**, 10490.
32 K. Kong, J. Liang, F. Cui, Y. Zhang, D. Yuan and R. Wang, *Chem. Eng. J.*, 2024, **502**, 157838.
33 X. Zhang, J. Liu, H. Zhang, Q. Zhang, J. Shen, Y. Wei and C. Wang, *Sep. Purif. Technol.*, 2025, **357**, 130039.